**THE EUROPEAN
PHYSICAL JOURNAL
SPECIAL TOPICS**

Review

Nanomotors

Mariana Alarcón-Correa[1,2], Debora Walker[1,2], Tian Qiu[1], and Peer Fischer[1,2,a]

[1] Max Planck Institute for Intelligent Systems, Heisenbergstr. 3, 70569 Stuttgart, Germany
[2] Institute for Physical Chemistry, Univ. Stuttgart, Pfaffenwaldring 55, 70569 Stuttgart, Germany

Abstract. This minireview discusses whether catalytically active macromolecules and abiotic nanocolloids, that are smaller than motile bacteria, can self-propel. Kinematic reversibility at low Reynolds number demands that self-propelling colloids must break symmetry. Methods that permit the synthesis and fabrication of Janus nanocolloids are therefore briefly surveyed, as well as means that permit the analysis of the nanocolloids' motion. Finally, recent work is reviewed which shows that nanoagents are small enough to penetrate the complex inhomogeneous polymeric network of biological fluids and gels, which exhibit diverse rheological behaviors.

1 Introduction

Active propulsion of swimming microorganisms bestows an evolutionary advantage by enabling microswimmers to outrun diffusion. Dusenbery has observed that the smallest motile genus of bacteria has a minimum length of 800 nm, i.e. almost a micron, while non-motile bacteria can be as small as 200 nm [1]. Active propulsion in bacteria is in general coupled to sensory mechanism, such as a chemo- or photo-tactic stimulus, which works if there are detectable concentration differences or gradients that the cell can sense. These sensory mechanisms in turn give rise to "size limits" for motile bacteria, that are indeed around a micron [1]. One may therefore conclude that active motion or swimming is absent at the nanoscale in living systems. Several well-studied motor proteins, however, do not simply diffuse, but actively move, albeit not in free space, but on tracks or when they are anchored to a supporting membrane [2]. These sophisticated enzyme-nanomachines are much smaller than motile bacteria and they have a typical size of ∼10 nm. This begs the question whether 'free' swimmers at the nanoscale are feasible and if so, what purpose active motion or enhanced diffusion may serve at this length scale?

Whether enzymes do indeed "swim" when they are catalytically active is a question that a number of research groups are beginning to address [3–5]. This minireview does not consider motor proteins or "anchored" nanomotors, but introduces aspects related to the study of "freely" diffusing and actively moving macromolecules and artificial nanoparticles and nanomotors. Since the experimental analysis of actively
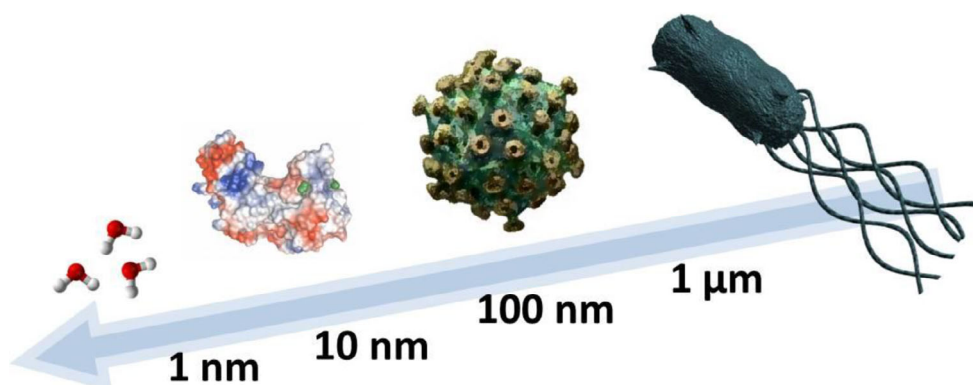
Fig. 1. Length scale and schematic depicting water molecules, an enzyme, a virus as well as a motile bacterium.

diffusing "nanoswimmers" is far from trivial, as the particles are well below the optical resolution limit, the minireview discusses a few experimental methods that can be used to observe potential nanoscale "swimmers", as well as experimental means to fabricate such structures. Some details regarding complex biological fluids, which are generally inhomogeneous and non-Newtonian, are given, and their influence on the behavior on sub-micron swimmers is discussed. This minireview is largely based on the published lecture note on the same topic [6] which is part of the summer school on "microswimmers – from single particle motion to collective behavior".

1.1 Insights from theory

The emphasis of this minireview is on truly "nano" nanomotors with characteristic lengths of 1 to 100 nm. Smaller than this are most (small) molecules (e.g. the sugar molecule lactose has an effective hydrodynamic radius of ∼0.3 nm), but proteins and nanoparticles are nano-sized (see Fig. 1). Whereas inorganic particles are readily visualized using electron microscopy, determining the size of proteins in solution is more difficult. Since most proteins have approximately the same density (about $1.37 \, g/cm^3$), it is possible to estimate their (minimum) dimension from their mass. The majority of proteins are small and consist of 250 to 400 amino-acids [7]. Since the average amino acid has a molecular mass of 100 Da, one obtains a size estimate of ∼2 nm. Some enzymes and motor proteins consist of several domains and are typically larger, with sizes of up to ∼20 nm. For the subsequent discussion it is necessary to determine if the concept of "swimming", which stems from continuum hydrodynamics, also applies to enzymes and nanoparticles. For a system that is reacting and described by non-equilibrium thermodynamics this is a difficult question. We therefore first consider a "passive" diffusing nanocolloid. For such a particle solvated by water, as shown in Fig. 2, fluctuations arise in the hydration shell, because water molecules constantly leave and enter the shell. A continuum description may be warranted if the fluctuations are small, say less than 10%. An enzyme with a characteristic length of 5 nm will already be surrounded by 50,000 water molecules in a layer as thin as one molecular diameter (more realistically at least 1 nm of water around a protein is typically part of the hydration shell). Assuming Poisson statistics, fluctuations of 10% mean that only about 100 water molecules are needed (on each side) for the object to be considered solvated by a continuum of fluid. This is a very small number of solvent molecules compared to the amount of solvent molecules that are found in the hydratation shell of an typical nanoswimmer.
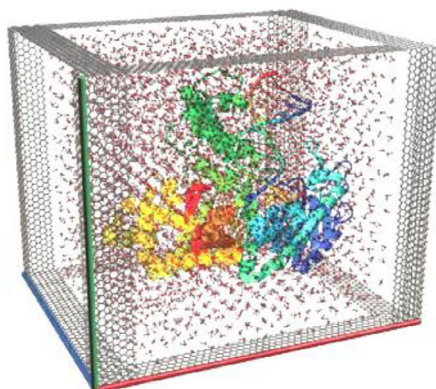
Fig. 2. Simulation box with enzyme surrounded by water molecules.

A word of caution is that the protein surface is rough and cannot simply be approximated by a smooth body. This is also the reason why it is not possible to use the Perrin friction factors to estimate the exact shape (aspect ratio) of ellipsoidal proteins from protein hydrodynamics studies. However, this does not affect the above arguments. One can thus conclude that even a nanoparticle can be described by continuum hydrodynamics. One might therefore also assume that "nanoswimmers" are described by continuum hydrodynamics, although this is an *assumption*, as there is currently no complete theoretical description of (the hydrodynamics) of a catalytically active nanoparticle. A theoretical treatment that considers the scaling behaviour of diffusiophoretic particles has recently appeared [5]. These authors conclude on the basis of particle-based simulations of chemically powered Janus $\sim$ nm motors that the principle of self-diffusiophoresis still operates at the nanoscale, even though the motion is subject to strong fluctuations [5].

1.2 Rheology of biological fluids

In general, biological fluids can be classified into three categories based on their rheological behavior: i) Viscous (Newtonian) fluids, for example cerebrospinal fluid, aqueous humor and urine can be considered as Newtonian fluids in most cases; ii) Viscoelastic liquids, the largest fraction of biological fluids, such as mucus, vitreous humor and synovial fluids; iii) Viscoelastic solids, for instance muscle, blood vessels and brain tissue. Fluids in the latter two categories are called non-Newtonian fluids in general, and most biological fluids fall into this category. Table 1 summarizes the rheological property of typical biofluids in the human body.

The diverse rheological properties encountered in biological fluids represent one of the major challenges to develop microdevices that are capable of propelling through them. Based on the rheology different swimming strategies will be effective. For example, we developed a highly symmetric single-hinge microswimmer, which takes advantage of shear-thickening or shear-thinning to break the time-reversal symmetry, and therefore lead to propulsion at low Reynolds number [8].

2 Experimental means to observe nanomotors

Most studies on microswimmers entail the observation of a few swimmers in an optical microscope and the analysis of their trajectories. Two experimental methods are briefly introduced below, which are well-established techniques that find use

Table 1. Rheology of selected biofluids.

No.	Name	Physiology	Fluid Model	Rheology
1	Whole blood	contains blood plasma, red and white blood cells	i) Shear thinning for $\dot{\gamma} < 50\,\mathrm{s}^{-1}$ ii) Newtonian for $\dot{\gamma}$ 50–1000 s^{-1}[9]	60 mPa·s at $0.1\,\mathrm{s}^{-1}$ 5 mPa·s at $50\,\mathrm{s}^{-1}$ 5 mPa·s at 50–1000 s^{-1} [10]
2	Blood plasma	92% water, 7% proteins, 1% salts, sugars, fats, hormones and vitamins	Newtonian [9]	$\sim$1.24 mPa·s [9]
3	Vitreous humor	a clear gel that fills the space between the lens and the retina, contains 99% water, 1% collagen and salts, sugars, and proteins	i) Viscoelastic [11] ii)Shear thining [12] iii) Depend on device size [13]	4 Pa·s at $0.15\,\mathrm{s}^{-1}$ [12]
4	Synovial fluid	expressed in joints to lubricate the articulating cartilage surfaces, contains hyaluronic acid, proteinases, and collagenases	Shear thinning	900 mPa·s at $1\,\mathrm{s}^{-1}$ 70 mPa·s at $250\,\mathrm{s}^{-1}$ [14]
5	Urine	secreted by the kidneys, stored in bladder and excreted through the urethra, contains about 93% of water at pH 6, remaining solids where the largest fraction is urea	Newtonian	0.85 mPa·s [15]
6	Gastric mucus	protects the stomach from low pH, complex contains water and high levels of hydrochloric acid in thelumen, complex fluid that contains glycoproteins and water	i) Shear thinning ii) Yield stress	6 Pa·s at $1.15\,\mathrm{s}^{-1}$ 0.5 Pa s at $23\,\mathrm{s}^{-1}$ [16]

in analysing the diffusion of enzymes and molecules, namely dynamic light scattering (DLS) and fluorescence correlation spectroscopy (FCS). Both techniques have a temporal resolution that permits the rotational diffusion time of a $\sim$10 nm particle to be resolved, such that their characteristic time scales can probe the persistence of nanoswimmers.

2.1 Dynamic light scattering (DLS)

In dynamic light scattering a laser passes through the sample and the scattered intensity is recorded. The diffusion of scatterers causes fluctuations in the signal. A correlation function (time correlation) of the scattered light can therefore be calculated. Knowing the size and the optical properties of the particles will provide a measure of the diffusion constant. If the particle is a nanomotor, then one should observe a reduction in the relaxation times when the particle, in addition to Brownian motion, undergoes self-diffusiophoresis. Standard software used by DLS instruments assumes that particles are passive and may therefore associate a reduction in the correleation as function (i.e. a "speed-up") with reduced hydrodynamic radius. In the case of inorganic particles the size of the particles can be determined using transmission electron microscopy, and a change in the relaxation time can then be interpreted as a change in the particle motility. A schematic of a DLS setup is shown in Fig. 3.
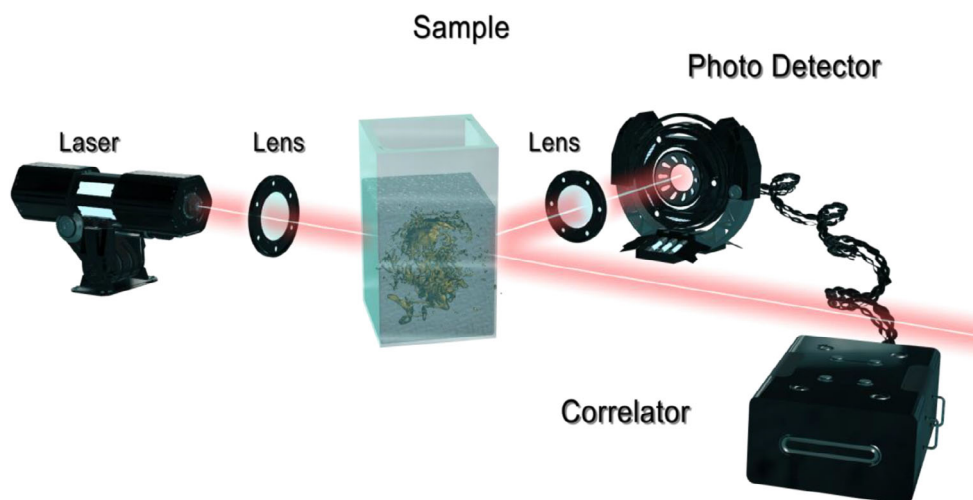
Fig. 3. Schematic depicting a light scattering setup. Light from a laser is focused into a sample containing the nanoparticles. A photodetector records the scattered light. The detector is either mounted on a goniometer or, more typically, is fixed (e.g. at $\sim 170°$) with respect to the incident beam. The signal is analysed by a fast correlator.

The relaxation rates Γ for the translational (tr) and rotational (rot) diffusion of a Stokes sphere with radius R are:

$$\Gamma_{tr} = D_{tr}q^2 = \frac{k_B T}{6\pi\eta R}q^2; \qquad q = \frac{4\pi n}{\lambda}\sin\left(\frac{\theta}{2}\right) \tag{1}$$

$$\Gamma_{rot} = 6\tau_{rot}^{-1} = \frac{6k_B T}{8\pi\eta R^3}, \tag{2}$$

where D_{tr} is the diffusion constant, η the viscosity, θ the scattering angle, n the refractive index, and λ the wavelength. The scattering vector (q) depends on the scattering angle and the wavelength [17]. The rotational and translational relaxation times appear both as exponents in the intensity autocorrelation functions and can therefore in general not be distinguished unless one uses polarized light scattering. However, for nanoparticles that are strongly anisotropic (e.g. rod-shaped) or smaller than 40 nm and optically anisotropic, it is indeed possible to see separate translational and rotational peaks [18,19]. In Fig. 8 this is shown for Janus nanomotors.

2.2 Fluorescence correlation spectroscopy (FCS)

FCS is a powerful technique to measure the diffusion of molecules, enzymes and small particles. In addition it permits the observation of conformational changes [20] or binding interactions [21]. Only small sample volumes and concentrations are required ($\sim$1 nM, $\sim$100 μl solution). The setup (see Fig. 4) is based on a confocal microscope. A laser is focused by a high N.A. objective into a sample of fluorophores or fluorescently labeled macromolecules that diffuse through the focal volume. The same objective collects the fluorescence signal. A fluorophore starts to emit light as soon as it enters the confocal volume and the fluorescence is detected until it leaves that
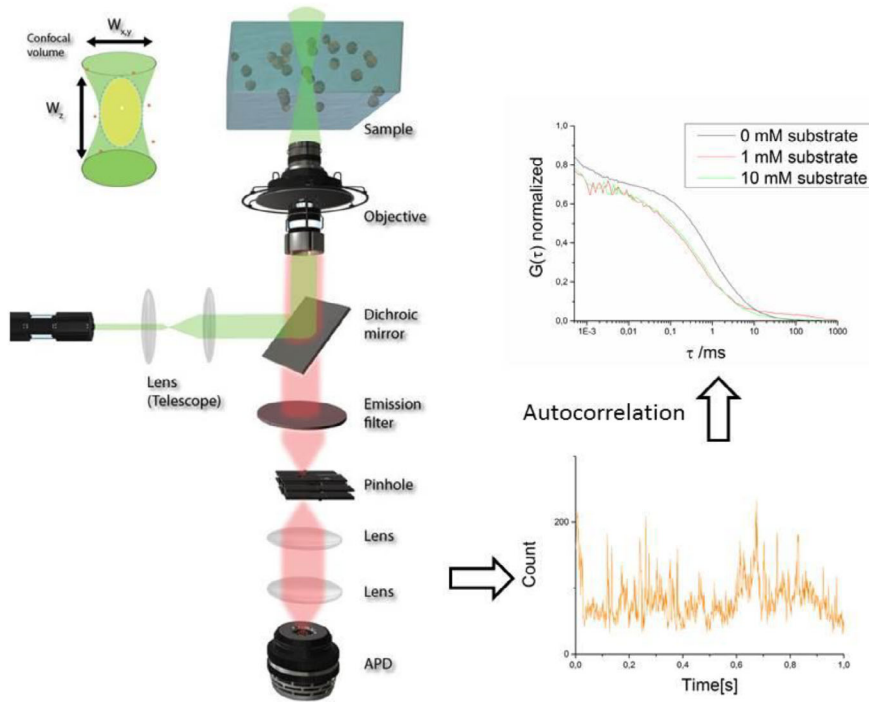
Fig. 4. Schematic setup of a Fluorescence Correlation Spectroscopy (FCS) measurement. The confocal volume is defined by the size-ratio of w_z/w_{xy}.

volume. A dichroic filter blocks most ($\sim$99%) of the scattered light. A pinhole and two lenses block the remaining scattered laser light and any out-of-focus fluorescence. The confocal volume is small (femtoliter) so that ideally only one fluorophore is detected at any time. An Avalanche Photo Diode (APD) can detect single photons with μs resolution. The signal is recorded as a time-trace (see Fig. 4, orange line). The duration of the photon burst is a measure of the diffusion time of the molecule or particle. An average diffusion time is obtained from the autocorrelation of the time trace.

The autocorrelation function $G(\tau)$ is defined by the product of the intensity at time t, $F(t)$ and the intensity after a time $t + \tau$, $F(t + \tau)$. These parameters are compared and averaged over a large number of measurements [22]:

$$G(\tau) = \frac{\langle F(t) \cdot F(t + \tau) \rangle}{\langle F(t) \rangle^2}. \tag{3}$$

In order to extract the diffusion time a specific model, G'(τ), is required for G(τ). Apart from the diffusion term this model also contains a term to correct for the fluorophore-specific triplet lifetime:

$$G^{'}(\tau) = G_D(\tau) \cdot G_T(\tau). \tag{4}$$

Comparison with a fluorophore that has a known diffusion constant permits the determination of absolute diffusion constants. As an example we consider a 250 kDa enzyme in the absence and in the presence of its substrate. The resulting measurements are shown in Fig. 4. The question why enzymes experience enhanced diffusion when catalytically active is as yet not fully understood [3,4].

3 Fabrication of nanomotors

Microswimmers have to break symmetry to move at low Reynolds number (for details, see minireview [23] by R.G. Winkler in this issue). This either calls for non-reciprocal body-shape changes or corkscrew motion in microorganisms. Self-phoretic particles whose shape is fixed also have to break symmetry in order to support a local gradient across the particle that gives rise to self-propulsion. Most artificial swimmers are therefore based on two-sided particles, also known as Janus particles that – just as the Roman god Janus – possess two faces, here with different chemical or physical properties on each of the hemispheres [24]. A local chemical reaction or physical change causes a gradient around the particle which induces the motion (for details, see minireview [25] by M. Popescu et al. in this issue).

A number of different fabrication methods have been developed and micron-sized Janus particles can be prepared by a great number of methods. However, the fabrication of Janus *nano*particles (JNPs) is still challenging, since most schemes to synthesize nanoparticles produce symmetric particles. In what follows, a brief survey of a few promising syntheses and fabrication methods to produce Janus particles is presented with emphasis on methods that can be used to fabricate JNPs in the size range between 10 and 100 nm.

3.1 Self-assembly of block-copolymers

By mixing two different block copolymers in the appropriate solvents, micelles are formed containing patches that can separate into two phases under the right conditions. This has been demonstrated for larger particles [26] and for dendrimer-based particles with a hydrodynamic radius of up to 20 nm [27]. The use of two branched polymers with different branches can also lead to the formation of patchy or Janus particles. For this to work, it is necessary that the polymers are highly incompatible and the solution conditions need to be adjusted and optimized in each case to carefully strike a balance between entropy (favoring mixing) and the enthalpy (favoring de-mixing) of the system [28].

If the self-assembling polymer structures are further modified, it is also possible to create a Janus structure where a cavity forms only on one side of the particle. Recently, it has been shown that if this cavity formation is combined with the entrapment of catalytically active particles, then the entire Janus structure becomes a self-propelling nanomotor [29]. For this PEG-PS copolymers are mixed to form vesicles in an organic solvent (1:1, THF:H_2O). Platinum nanoparticles are mixed into the solution and the organic phase is slowly evaporated. As the solvent evaporates, the vesicles deform into bowl-shaped structures (stomatocytes) and entrap the platinum nanoparticles. Under carefully chosen conditions the resulting particles will have a large enough opening to allow the diffusion of H_2O_2 in and out of the cavity, while preventing the escape of the catalytic Pt-nanoparticles. The platinum inside the stomatocytes catalyzes the decomposition of H_2O_2 into H_2O and O_2 and so the autonomous movement of the stomatocytes can be controlled by changing the H_2O_2 concentration [30].

3.2 Reactions at a liquid interface

The use of an interface to induce symmetry breaking is one of the most efficient and commonly used methods to grow JNPs. While the following reactions do not appear to have been used to synthesize active JNP nanomotors, it should be possible to modify the schemes accordingly.
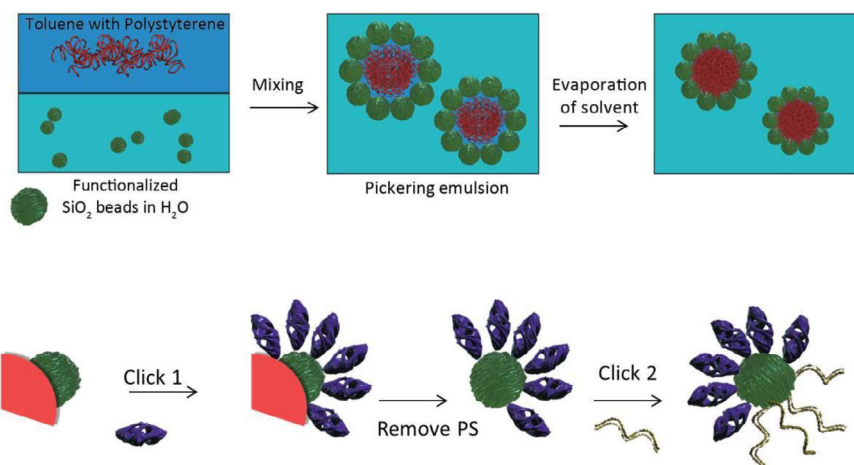
Fig. 5. Mixing polystyrene with functionalized silica particles, in a mixture of toluene and water provides a template for transforming the silica particles into silica Janus nanoparticles. See text for details. Image adapted from [31].

One of the most commonly used liquid-liquid interfaces are those formed in Pickering emulsions: An oil-water interface is stabilized by the presence of colloidal particles at the interface. The emulsion stability increases for larger particle size and this is a challenge if one wants to synthesize ($<100\,\mathrm{nm}$) JNPs, but it is possible, if the emulsion conditions are carefully controlled [30]. Using a water-toluene interface for instance permits the modification of silica nanoparticles (NPs). First, the NPs are surface-functionalized with an azide group and then dispersed in the aqueous phase and mixed with a solution of polystyrene is dissolved in toluene. Under sonication a Pickering emulsion forms. The toluene is removed under a slight vacuum. The silica particles are on one side in contact with the polystyrene and on the other with the aqueous solution. A twostep click reaction can then be used to form silica JNPs, for instance by first coupling biotin on the water side followed by the coupling of polyethylene oxide on the opposite side after removal of the polystyrene [31]. The process is schematically depicted in Fig. 5.

Another liquid interface system that results in JNPs ($\sim150\,\mathrm{nm}$) is the polymerization of a hydrophobic monomer in water in the presence of a colloidal surface. First, a micelle forms on the surface of the support colloidal particle while the polymerization occurs. The newly formed JNPs are automatically released after the larger particle sediments. By sonicating and adding a surfactant (sodium dodecyl sulfate) to the supernatant the formation of aggregates can be suppressed and single JNPs can be obtained [32].

3.3 Growth on a solid surface

Particles that adhere to a solid surface can be modified to form Janus particles. The range of possible modification techniques includes microcontact printing, UV-photopolymerization, plasma treatment, electrochemical and electroless growth of metals, and physical vapor deposition (e.g. sputtering), to name but a few examples. Most of these methods, however, do not work well enough when growing nanometer ($<100\,\mathrm{nm}$) sized Janus particles. At these small scales, for instance, chemical modification only works when the particles are closely packed and the molecules
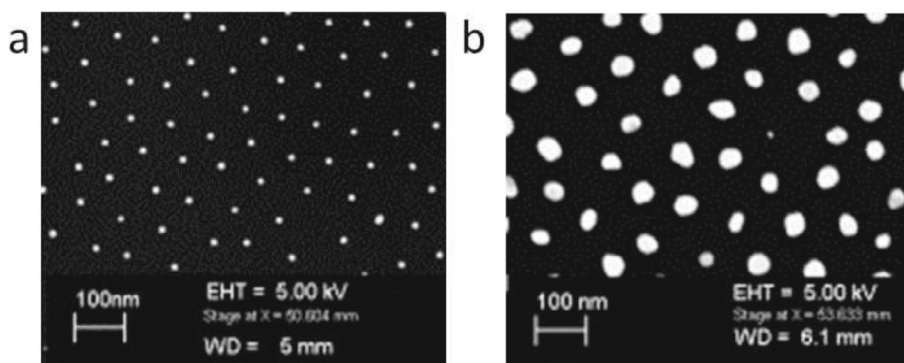
Fig. 6. Electron microscopy images of (a) AuNP arrays grown in our lab using BCML; (b) Same array after electroless deposition of silver. The size of the NPs is approximately 8 nm before growth (a) and then increased to 30 nm after growth.
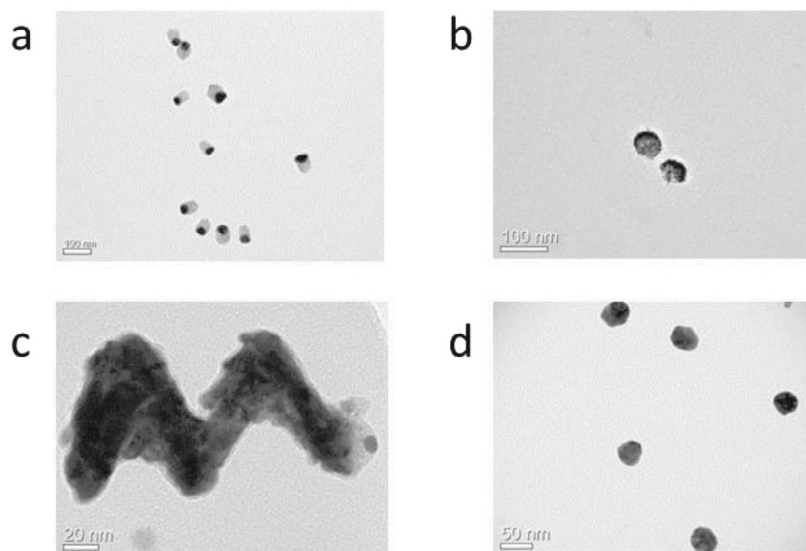
Fig. 7. TEM images from our lab of nanoGLAD-fabricated Janus nanoparticles. (a) 60 nm SiO_2-Au. (b) 50 nm Au-Pt. (c) 150 nm helical structure. The Au seed is visible followed by SiO_2 and the body of the helix is made by co-depositing Au and Fe. (d) 30 nm Pt-Au. When placed in a H_2O_2 solution these nanoparticles self-propel.

used for the modification are of considerable size (polymers). Under these conditions a UV-induced polymerization reaction was successfully used to photograft SiO_2 particles [33].

Electroless deposition of metals on surface-attached nanoparticles has, similarly, been shown to work at the nanoscale. This is relevant in the context of nanomotors, as metallic Pt is a favoured catalyst for self-phoretic particles, and gold is used for temperature-induced phoretic processes. Briefly, a Si wafer is patterned with nanoparticles using block copolymer micellar nanolithography (BCML) [34]. The metal salts are reduced on the surface after being dissolved in an organic solvent together with a block copolymer. It is possible to use different metal salts for the process and thus to obtain a variety of metal nanoparticles (Au, Pt, Ni, etc.) on the surface. Subsequently, the surface is washed to ensure that the electroless growth will only take place on

2250The European Physical Journal Special Topics
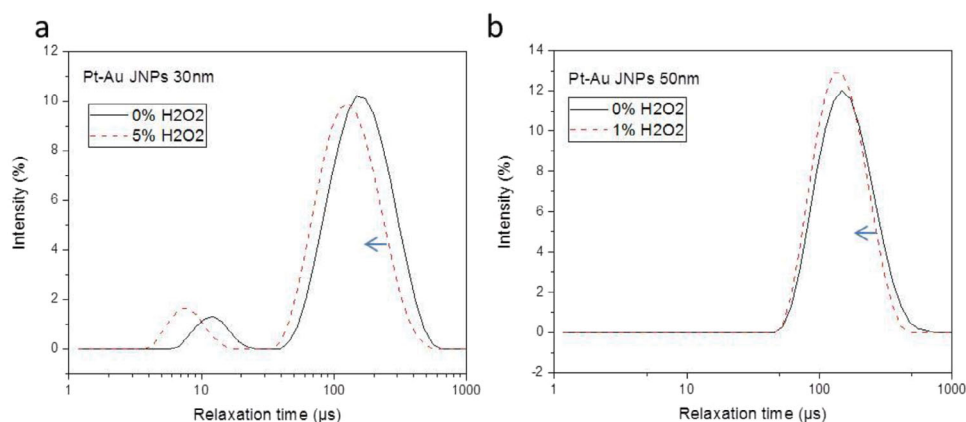
Fig. 8. DLS measured relaxation times of (a) 30-nm Pt-Au JNPs and (b) 50 nm Pt-Au NPs, both in water and in 5% H_2O_2 solutions. A shift in the relaxation peaks is observed (marked by the arrows).

the metal NPs. A diluted Tollens reagent solution is mixed with an aqueous solution of glucose and then poured over the patterned surface. The thickness of the silver layer is determined by the duration of the growth process. The sample surface is then washed and dried to stop the growth process [35].

While it is in principle possible to sputter onto NPs that have been previously deposited on a solid substrate, the evaporant will then also decorate the empty areas of the substrate and thus generate nanosized debris, which is hard to separate from the coated JNPs. For this reason a physical vapor deposition at an oblique angle is a preferred method for fabricating truly nanoscale homogenous JNPs in high yield. Particles are dried or deposited onto a substrate, preferably as a monolayer, and then coated in a vacuum chamber. A thermal or electron-beam source heats the material that is to be deposited, which makes this a very versatile method. Recently mesoporous silica nanoparticles have been coated with Pt and shown to propel in H_2O_2 solutions. The mesoporous nanoparticles offer the opportunity to load the silica particles with drugs or other substances [36].

A particular variant of a shadow-growth physical vapor deposition method is glancing angle deposition (GLAD), where it is possible to angle and rotate the substrate during deposition to localize and shape the deposited material. Particularly homogenous Janus nanoparticles can be obtained when the surface contains a well ordered layer of seed particles. If a substrate is used that has been fabricated with the BCML method (seeds of ∼10 nm), then it is possible to fabricate JNPs [37]. If the substrate is also cooled, then even highly mobile adatoms can be deposited, and Janus nanoparticles with complex non-spherical shapes can be produced [37].

Inclusion of Pt in these kinds of JNPs permits the realization of nanomotors. Placed in a H_2O_2 solution the platinum catalyzes the decomposition of H_2O_2 into H_2O and O_2 and thus induces autonomous motion [19]. This motion can be observed using DLS (see 2.1). Figure 8 shows DLS measurements for two different-sized JNPs in water and in H_2O_2 solutions, respectively. In the case of the 30 nm Pt-Au JNPs a separate rotational peak is observable.

4 Biological fluids

Many applications that have been suggested for artificial micro- or nanomotors and propelling particles are of a biological or medical nature and thus require efficient
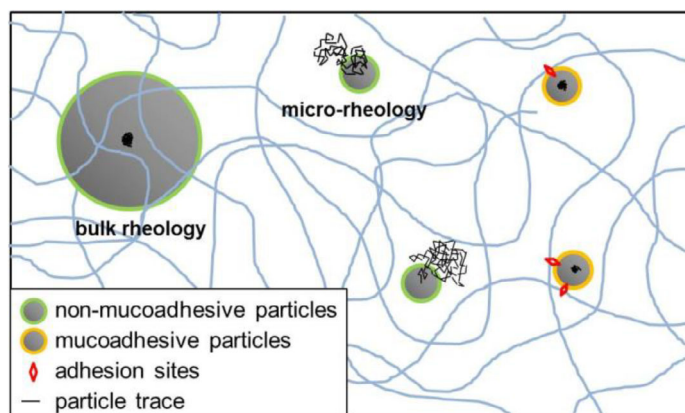
Fig. 9. Schematic of the length scale dependence of rheological measurements in viscoelastic polymeric gels. As the particle size increases beyond the pore size of the mesh, its movement becomes hindered by the polymer matrix and the perceived viscoelasticity increases. Adhesion to the polymer chains can furthermore increase the measured viscoelasticity dramatically.

navigation and stability inside not only water and simple aqueous salt solutions, but also in more complex biological fluids and tissues. Biological fluids are generally inhomogeneous and non-Newtonian, which increases the complexity of operating artificial microswimmers. In some cases these media can provide simpler means for actuating such swimmers [38]. An example of the rheology and motion of nanostructures through a complex biological model fluid, hyaluronan (HA), is presented, before some general properties of biological non-Newtonian fluids are tabularized.

HA is a linear polysaccharide that is formed in the cell's plasma membrane and occurs in low concentrations in almost all biological fluids and tissues, in particular the synovial fluid of the joints and the vitreous of the eye [39]. A very characteristic feature of HA solutions is their high viscosity even at very low concentrations. At higher concentrations HA forms a highly viscoelastic interconnected 3D transient network [40].

Associated with this network is a pore size, which is roughly on the order of tens of nanometers [40,41]. The pore structure leads to strongly size-dependent transport properties of particles at that length-scale. Microrheology can be used to examine the material's physical properties as experienced by very small particles. On a microscopic scale the mechanical properties of a fluid can be highly heterogeneous and differ significantly from the average bulk values. This is illustrated in Fig. 9, where a schematic representation shows how the choice of probe size and surface properties affects the measurement of the mesh's viscoelastic properties and the particle diffusion.

In the following an example of an externally driven magnetic nanopropeller is used to penetrate biological gels and to illustrate the dynamics in an inhomogeneous non-Newtonian gel. A nanopropeller is an artificial cork-screw like structure (see Fig. 10) that contains a magnetic moment perpendicular to the long axis of the propeller. Magnetic nanopropellers can be fabricated using the nanoGLAD method described in Sect. 3.3. It is advantageous to use a larger seed particle spacing of >100 nm. The size of the Au-seeds can then be enlarged, before growing a magnetic nickel section (40 nm). The body of the helices can be grown with silica. The nanohelices can be functionalized with quantum dots to render them visible in the optical microscope.

A weak rotating magnetic field will exert a torque on the magnetic moment and rotate the propeller. Due to translation-rotation coupling the propeller is drilled through the medium [42].
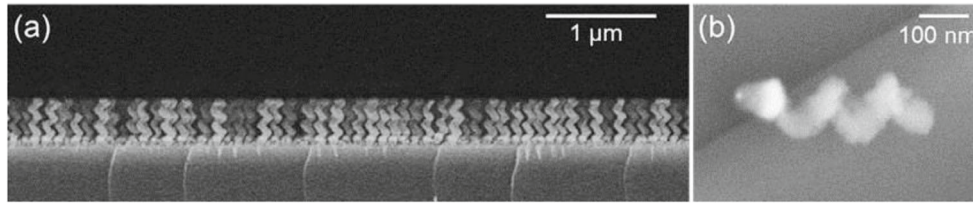
Fig. 10. SEM images of the nanoGLAD propellers: (a) side view on wafer and (b) close-up of one nanohelix with both the Au-dot and the Ni-section clearly visible. The helices have a filament diameter of roughly 70 nm and the resulting structures are approximately 400 nm long. The image was taken with an SE2 detector. Image reprinted from Ref. [42]. (This figure is subject to copyright protection and is not covered by a Creative Commons license.)

4.1 Size requirements and Péclet number

The Péclet number Pe is defined as the ratio of directional to diffusive motion and reflects the propeller's ability to perform the kind of deterministic translational motion necessary for precise tetherless control. It can be used to determine the minimum length of a propeller that still allows for directional propulsion under the respective conditions. A diametrically magnetized helix is considered with a magnetic moment m subject to rotation by an external magnetic field of strength H and frequency ω. In the absence of Brownian diffusion the propeller frequency matches that of the magnetic field, and the helix's axis is aligned with the rotation axis of the field. Rotation-translation coupling leads to a translational velocity.

Thermal noise may affect the motion *via* three different mechanisms: (i) hindering of the forced rotation about the axis (*i.e. via* rotational diffusion about the helix axis); (ii) hindering the propulsion *via* translational diffusion along the axis, which perturbs the translational velocity; and (iii) reduction of directionality by introducing misalignment in the angle the axis of the helix makes with the rotation axis of the field (*via* rotational diffusion of the helical axis). Mechanisms (i) and (ii) directly affect the propulsion speed, but not the directionality; (iii) affects the directionality or steerability. All of the above mechanisms are characterized by their respective Péclet numbers (Pe) [42]. The criterion for the minimal size of a propeller can be derived from the condition that Pe = 1, at which point diffusion becomes equal to the rate of directed motion. Based on these expressions Leshanski and Morozov have determined the critical helix length, above which the external driving force is more important than the noise [42]. Importantly, the critical length associated with the steerability is not affected by the fluid viscosity at frequencies significantly below the step-out frequency, where one obtains a simple condition for the steerability (see Ref. [42] for details):

$$Pe^{\perp}_{r*} \approx \frac{mH}{2k_BT} > 1. \tag{5}$$

Given the geometry of the nanohelices and driving frequency one can estimate the minimum "stable" dimensions. For a four-turn propeller screw with a helix to filament radius ratio of 1, it was found numerically that the minimum length in water is $\sim 1\,\mu$m at a driving frequency of 50 Hz. These estimates support experimental observations indicating that thermal fluctuations hinder propulsion of 400 nm nanohelices in water. Increasing the viscosity to $\eta = 25$ cP, the critical lengths are reduced to ~ 350 nm. Steerability under these conditions for realistic values of the magnetic moment is retained.

It is observed that for 5 mg/mL HA no micropropeller translates through the gel. The nanoscrews on the other hand, in addition to displaying a higher step-out

frequency than the larger helices in the purely viscous fluid, actually seem to experience a considerable enhancement in propulsion when moved from the viscous into the viscoelastic medium. Measurements of the propulsion speed suggest that the nanoscrews do not experience the macroscopic viscosity of the polymer solution, since their step-out frequency does not, as for the larger propellers, decrease. At the same time the nanopropellers retain very high directionality and show high (dimensionless) velocities.

The reversal of relative efficacy between microhelices in the Newtonian medium and nanohelices in HA is a general consequence of the mesh network present in biological fluids. In a Newtonian fluid, the magnetic torque that can be applied to a nanopropeller, and the viscous drag that opposes it both scale as L^3, where L is the characteristic particle size. Translational diffusion on the other hand scales as L^{-1}. The net result is that larger particles propel with improved efficiency in a Newtonian fluid. In the mesh network of HA, however, the resistance to motion ζ, is associated with an activation barrier determined by the elastic expansion of the mesh [41, 43]:

$$\zeta \approx \zeta_0 \exp\left(b\left(L/\psi\right)^c\right). \tag{6}$$

Here, ψ is the mesh size, and ζ_0 is the resistance in pure solvent. b approaches 1, and c is usually assumed to be 1 [41]. Since this grows much faster with size than the cubic term in the torque, it means that in biological fluids comprised of dense networks, increasing the particle size only improves propulsion efficacy for propellers up to around the critical mesh size, which decreases again for larger particles.

These observations show that it is advantageous to be at the nanoscale for actively driven motion through inhomogeneous biological networks.

5 Conclusions

Symmetric "active" motion can lead to enhanced diffusion [44, 45], but a *swimmer* needs to break symmetry to overcome the constraints of kinematic reversibility at low Reynolds number. This calls for special "asymmetric particles". The synthesis and assembly of such low symmetry nanostructures and Janus nanoparticles is briefly surveyed. Janus (nano)particles can by virtue of their broken symmetry support a local concentration, charge, or temperature gradient that is established across the particle itself. This gradient causes, respectively, self-diffusio-, -electro- or -theromophoresis. In principle, these concepts may also apply to catalytically active macromolecules (enzymes). The diffusion of nanoswimmers can be measured using dynamic light scattering and fluorescence correlation spectroscopy. Actively moving and externally controlled nanoagents are small enough to penetrate the complex inhomogeneous polymeric network of biological fluids and gels, which exhibit diverse rheological behaviors.

References

1. B. Dusenbery, *Living at the Microscale* (Harvard University Press, 2009)
2. R.D. Vale, R.A. Milligam, Science **288**, 88 (2000)
3. S. Sengupta, et al., J. Am. Chem. Soc. **135**, 1406 (2013)
4. C. Riedel, et al., Nature **517**, 227 (2015)

5. P.H. Colberg, S.Y. Reigh, B. Robertson, R. Kapral, Acc. Chem. Res. **47**, 3504 (2014)
6. M. Alarcon-Correa, P. Oswald, T. Qiu, D. Walker, P. Fischer, C5 Nanomotors, in Lecture Notes of the DFG SPP Summer School 2015, edited by G. Gompper et al., Schriften des Forschungszentrums Jülich, Key Technologies. 110 (Forschungszentrum Jülich, 2015)
7. H.P. Erickson, Biological Procedures Online **11**, 32 (2009)
8. T. Qiu, et al., Nat. Commun. **5**, 5119 (2014)
9. R. Roselli, K. Diller, *Biotransport: Principles and Applications*, Ch. 4 (Springer, 2011)
10. R.L. Whitmore, *Rheology of the Circulation* (Pergamon Press, 1968)
11. J. Pokki, et al., *Conf. Proc. IEEE Eng. Med. Biol. Soc.* 2813 (2012)
12. S. Suri, R. Banerjee, Trends Biomateri. Artif. Organs **20**, 72 (2006)
13. T. Qiu, et al., *IEEE Int. Conf. on Robotics and Automation (ICRA)* 3801 (2014)
14. B.P. Conrad, Master Thesis, University of Florida (2001)
15. J. Kienlen, et al., Ann. Fran. Anesth. Reanimation **9**, 495 (1990)
16. D.C. Markesich, B.S. Anand, G.M. Lew, D.Y. Graham. Gut. **36**, 327 (1995)
17. B.J. Berne, R. Pecora, *Dynamic Light Scattering with Applications to Chemistry, Biology and Physics* (Dover, 1976)
18. J. Rodriguez-Fernandez, et al., J. Phys. Chem. **111**, 5020 (2007)
19. T.-C. Lee, et al., Nano Lett. **14**, 2407 (2014)
20. H. Chen, et al., Proc. Natl. Acad. Sci. **25**, 10459 (2007)
21. S. Hou, et al., Laser Phys. Lett. **11**, 085602 (2014)
22. J.R. Lakowicz, *Principles of Fluorescence Spectroscopy* (Springer, 2006)
23. R.G. Winkler, Eur. Phys. J. Special Topics this issue (2016)
24. C. Casagrande, M. Veyssie, C.R. Acad. Sci. (Paris) **306**, 1423 (1988)
25. M. Popescu, W. Uspal, S. Dietrich, Eur. Phys. J. Special Topics **225**, 2189 (2016)
26. D.A. Christian, et al., Nat. Mater. **8**, 843 (2009)
27. X. Feng, et al., J. Am. Chem. Soc. **130**, 11662 (2008)
28. Y. Chang, et al, Macromolecules **38**, 6201 (2005)
29. D.A. Wilson, et al., Nat. Chem. **4**, 268 (2012)
30. A. Perro, et al., Colloids Surf. A **332**, 57 (2009)
31. J. Zhang, et al., Chem. Mater. **21**, 4012 (2009)
32. L. Nie, et al., Angew. Chem. Int. Ed. **46**, 6321 (2007)
33. L. Liu, et al., Langmuir **25**, 11048 (2009)
34. R. Glass, et al., Nanotechnology **14**, 1153 (2003)
35. S. Kruss, et al., Langmuir **28**, 1562 (2012)
36. X. Ma, K. Hahn, S. Sanchez, J. Am. Chem. Soc. **137**, 4976 (2015)
37. A.G. Mark, et al., Nat. Mater. **12**, 802 (2013)
38. T. Qiu, et al., Nature Commun. **5**, 5119 (2014)
39. M.K. Cowman, S. Matsuoka, Carbohydr. Res. **340**, 791 (2005)
40. A. Masuda, et al., J. Am. Chem. Soc. **123**, 11468 (2001)
41. S.C. De Smedt, et al., Macromolecules **27**, 141 (1994)
42. D. Schamel, et al., ACS Nano **8**, 8794 (2014)
43. P.-G. de Gennes, *Scaling Concepts in Polymer Physics* (Cornell University Press, 1979)
44. E. Lauga, Phys. Rev. Lett. **106**, 178101 (2011)
45. P. Mandal, A. Ghosh, Phys. Rev. Lett. **111**, 248101 (2013)